Food Research International 120 (2019) 196–208

Contents lists available at ScienceDirect

Food Research International

journal homepage: www.elsevier.com/locate/foodres

Selective laser broiling of Atlantic salmon

Jonathan David Blutinger[a,*], Yorán Meijers[a,b], Hod Lipson[a]

[a] Columbia University, 500 W 120 St, New York, NY 10027, USA
[b] Wageningen University, 6708 PB, Wageningen, The Netherlands

ARTICLE INFO

Keywords:
Laser cooking
Blue laser
Protein denaturation
Heat penetration
Atlantic salmon
Mirror galvanometer
Food printing
Color

ABSTRACT

Selective laser broiling is a novel food processing technique that utilizes a 2-axis mirror galvanometer system to direct laser power to cook raw food. Unlike conventional cooking processes, laser cooking benefits from the high spatial and temporal precision of power delivery. In this investigation, we use a trochoidal scanning pattern to optimize the cooking of Atlantic salmon (*Salmo salar*), which is used as a model food system. We vary geometry of the trochoidal cooking pattern (circle diameter, circle density, and period) as well as the heat flux (2.71 MW/m^2 and 0.73 MW/m^2) and power (2 W and 5 W) of the blue laser and measure the internal temperature and depth of heat penetration via color analysis. Heat generated by blue laser operating at 445 nm has a thermal penetration depth nearing 2 mm in salmon and provide sufficient protein denaturation for cooking thin food layers. We achieve food safe cooking temperatures (> 62.8 °C) in the salmon fillets and desirable color and textural changes through the use of high speeds and repetitive exposure. Ultimately, the goal of this study is to explore laser cooking of meat with an eye to applications both in food printing as well as an augmentation of conventional oven cooking.

1. Introduction

Laser broiling—similar to broiling, which involves cooking via application of high radiative heat (Datta & Rakesh, 2013)—is a new cooking process where one or multiple lasers are used to heat food for human consumption (Singh, 2011). Laser cooking differs from conventional cooking methods in that it allows for a greater degree of temporal and spatial control of heat delivery (Blutinger et al., 2018b). Selective laser broiling (SLB) uses software to drive the specific temporal and spatial pattern of the laser beam. In this paper, we use a set of high-fidelity mirror galvanometers to precisely control the trajectory and speed of a 2 W and 5 W blue (445 nm) laser beam and study its application to the cooking of salmon. Since no prior research exists on the laser cooking of salmon our goal is to characterize the cooking effect and to identify potential use cases.

While laser cooking can be used to process most foods, it is particularly favorable for food produced using 3D printing. Food layered manufacture (FLM) (Zoran & Coelho, 2011)—an application of 3D printing—specifically refers to multi-ingredient food products that are additively constructed from puréed constituent materials (Hertafeld et al., 2018; Lipson & Kurman, 2013; Lipton, Cutler, Nigl, Cohen, & Lipson, 2015) and can be used to create nutrient-specific meals for consumers (Sun, Zhou, Yan, Huang, & Lin, 2018; Yang, Zhang, & Bhandari, 2017). A key challenge for conventional food printing is that printed constructs remain raw (uncooked), or require some degree of post-hoc cooking. To take full advantage of software-driven selective deposition of ingredients afforded by food printing, we explore the use of selective cooking with lasers since the power delivery and precision are unmatchable.

Understanding the heating effects of lasers is important for the laser cooking of meat, where specific temperatures must be reached to ensure safe consumption. For fish, the USDA requires a minimum internal temperature of 62.8 °C (145 F) for food safety (USDA FSIS, 2015). During the heating of salmon, various processes occur including textural changes, discoloration, and the protein denaturation of various protein groups (Bircan & Barringer, 2002; Ofstad et al., 1996). Because a blue laser has a high transmittance in water (Pope & Fry, 1997) it can provide deeper heat penetration for sub-surface cooking than an infrared laser which is more tailored for browning (Blutinger et al., 2018a; Sandu, 1986). Due to the high transmittance by water at 445 nm (Pope & Fry, 1997) and the high water content of salmon (69%) (USDA, 2018) deeper heat penetration should be expected when cooking with shorter wavelengths than conventional IR heat (Lentz, Pesheck, Anderson, DeMars, & Peck, 1995).

Cooked food, however, should not only be safe for consumption—its visual appeal and texture are just as important (Barbanti & Pasquini,

* Corresponding author.
E-mail addresses: jdb2202@columbia.edu (J.D. Blutinger), hod.lipson@columbia.edu (H. Lipson).

https://doi.org/10.1016/j.foodres.2019.02.043
Received 23 October 2018; Received in revised form 20 February 2019; Accepted 21 February 2019
Available online 23 February 2019
0963-9969/

2005; Yagiz et al., 2009). Both color (Barrett, Beaulieu, & Shewfelt, 2010; Jeremiah, Carpenter, & Smith, 1972; Sigurgisladottir et al., 1999) and perceived health-related benefits associated with the food product can greatly influence the degree of consumer acceptance (Anderson, 2001; Gormley, 1992). Particularly for animal protein (Mancini & Hunt, 2005) there is a strong association between color preference and purchasing intent (Carpenter, Cornforth, & Whittier, 2001); salmon farmers recognize this and will even add astaxanthin to their fish feed to ensure that their fish achieve the desired reddish-pink coloration (Dissing, Nielsen, Ersbøll, & Frosch, 2011). During heating, proteins denature (Haard, 1992) and change the muscle color from red to pale pink. We used a CIE $L^*a^*b^*$ color model, commonly used to assess visual changes in salmon, that measures lightness (L^*), redness (a^*) and yellowness (b^*) compared throughout the heating process (Kong, Tang, Rasco, Crapo, & Smiley, 2007).

We previously investigated the heating characteristics of a blue laser (Blutinger et al., 2018b) and a CO_2 laser with dough (Blutinger et al., 2018a; Chen et al., 2019), while Fukuchi, Jo, Tomiyama, and Takao (2012) use an IR laser cutter to process the fat portion of bacon. We envision future cooking systems that use multiple lasers at multiple wavelengths. For example, the tile of salmon presented in the Graphical Abstract was cooked using a blue laser and "grill" marks were added with an IR laser. Laser cooking technology could also be used in tandem with other cooking processes such as microwave and RF radiation, electric heating elements, gas fire, and infrared lamps to provide more targeted surface-level cooking.

In this study, the objective is to identify optimal parameters to fully cook salmon at the approximate layer thickness used in typical food printing (~2 mm). Salmon fillets are exposed to a trochoidal laser cooking pattern with parameters including circle diameter, circle density, number of repetitions, and period of the trochoid altered during each experiment. A 2 W and a 5 W blue diode laser are used to assess the effect of laser energy flux on the laser cooking of salmon. Software-controlled mirror galvanometers control the shape and speed of the trochoidal laser cooking pattern while color, thermal penetration, and internal temperature are measured from the heated samples.

2. Materials and methods

2.1. Sample preparation

Prior to commencing the experiments, store brand Atlantic salmon (*Salmo salar*) fillets were purchased at the local supermarket (Morton Williams, New York, USA). Fillets were placed in the freezer prior to cutting since the soft muscle protein made it difficult to thinly slice the meat. Once the meat was frozen, it was cut into thin slices (perpendicular to the skin) that were subsequently used for laser processing. It should be noted that reproducibility of quality measurements might be affected by the heterogeneity within each salmon fillet that could not be controlled in these experiments. In the present study, focusing on packaged salmon, a protein content of 20% and fat content of 6% can be assumed, based on the USDA standards (USDA, 2018).

2.2. Laser cooking apparatus

A custom mount was designed and 3D-printed to properly position the laser diode in front of the mirror galvanometers—henceforth referred to as "galvo mirrors"—(Fig. 1). Mounting holes were made in the printed fixture to facilitate precise positioning of the laser with respect to the galvo mirrors. Holes for the laser and galvo mirrors were slotted to allow for manual alignment of the two components with respect to one another.

2.2.1. Laser diodes

Throughout the course of the study, two lasers—a 2 W blue diode laser (J Tech Photonics, Inc., Kemah, USA) and a 5 W blue diode laser (Sunwin Technology Co., Guangzhou, China)—were utilized. Each laser operates at the 445 nm wavelength, while differing in the total output power, beam divergence, and diode size. The lower-powered (i.e., 2 W) blue laser produces a more collimated beam and is about ten times smaller than the 5 W laser diode, which is characterized by a higher beam divergence and a shorter focal length (18 mm). We use this difference in beam collimation as a way to compare the effect of beam flux on the laser cooking of salmon.

2.2.2. Hardware and galvo mirror control

In the present study, an Elegoo Uno R3 microcontroller (Elegoo Inc., Shenzhen, China) was used to determine the angle of the galvo mirrors and thus achieve the desired cooking patterns. The digital output signal from the Uno is within the 0–5 V range and the motors controlling each mirror accommodate voltage variation from −12 V to + 12 V, thus allowing full range of motion. Therefore, output from the microcontroller was converted to an analog signal via two 12-Bit DAC converters (MCP4725, Adafruit, New York City, USA) prior to being amplified by a custom-fabricated amplifier to 24 V, which was sufficient to provide full motion range for the mirrors. This amplified analog signal was then transmitted to each galvo mirror. In essence, the software and hardware framework allowed the motion of each mirror to be precisely controlled by converting a 12-bit analog value (0–4095) to a voltage (in the −12 V to + 12 V range) that translates to a mirror angle between 34° and 58°, as shown in Fig. 2(B).

2.2.3. Calibrating the galvo mirrors

Prior to SLB, the galvo mirrors needed to be properly calibrated in order to determine the degree of pincushion distortion—a type of deviation from rectilinear projection—as shown in Fig. 2(A). Considering the greatest permissible span of the reflected laser beam and the 3D-printed mounting fixture, an operating region was determined for the galvo mirrors. This region corresponded to 1500–2500 increments (inc) in the x-direction and 0–2500 inc in the y-direction for the 2 W laser, while 1000–3000 inc and 0–3000 inc were possible, respectively, for the 5 W laser. These cooking regions were also strategically selected to correspond to an analog value of 2048 (half of the 12-bit analog value range), since this analog value is closest to the laser beam's optical axis where rectilinear distortion is minimized.

Once a safe cooking region was established, both scaling and correction factor were calculated to determine how the analog values (0–4095) correspond to the x and y coordinates on the cooking platform. The x-axis was defined as running parallel to the direction of the beam as it exits the laser diode. The mirrors were set to various static positions within the operating region and measurements were taken using digital calipers to determine the laser beam movement based on analog value. Laser marks were etched onto the acrylic cooking plate at 500 inc intervals along both axes. The x scaling factor (s_x) was 68.5 inc mm^{-1} and the y scaling factor (s_y) was 88.8 inc mm^{-1}. The ratio of these scaling factors (68.5/88.8 = 0.82) was used to skew the size of the interlaced circles such that the produced pattern more closely resembled a propagating circle, as opposed to an ellipse.

2.2.4. Calculating laser-cooking energies

To parameterize the SLB of salmon more effectively, a trochoidal cooking pattern shown in Fig. 2(C) was chosen, as it allowed laser energy density and energy variance to be easily adjusted by changing the diameter and density of circles produced by the laser beam, as well as the speed of laser travel across the sample. Computer code was written such that five variables—circle radius, increment, scale, circle step, and time delay—could determine the corresponding energy per area (ω, J m^{-2}), energy per travel (ψ, J m^{-1}), speed (v, mm s^{-1}), frequency of oscillation (f, Hz), period (T, s), and circle density (ρ, rev mm^{-1}) of the trochoidal cooking pattern. In calculating these derived variables, laser power was assumed to remain constant during sample exposure to laser energy and pincushion distortion from the galvo

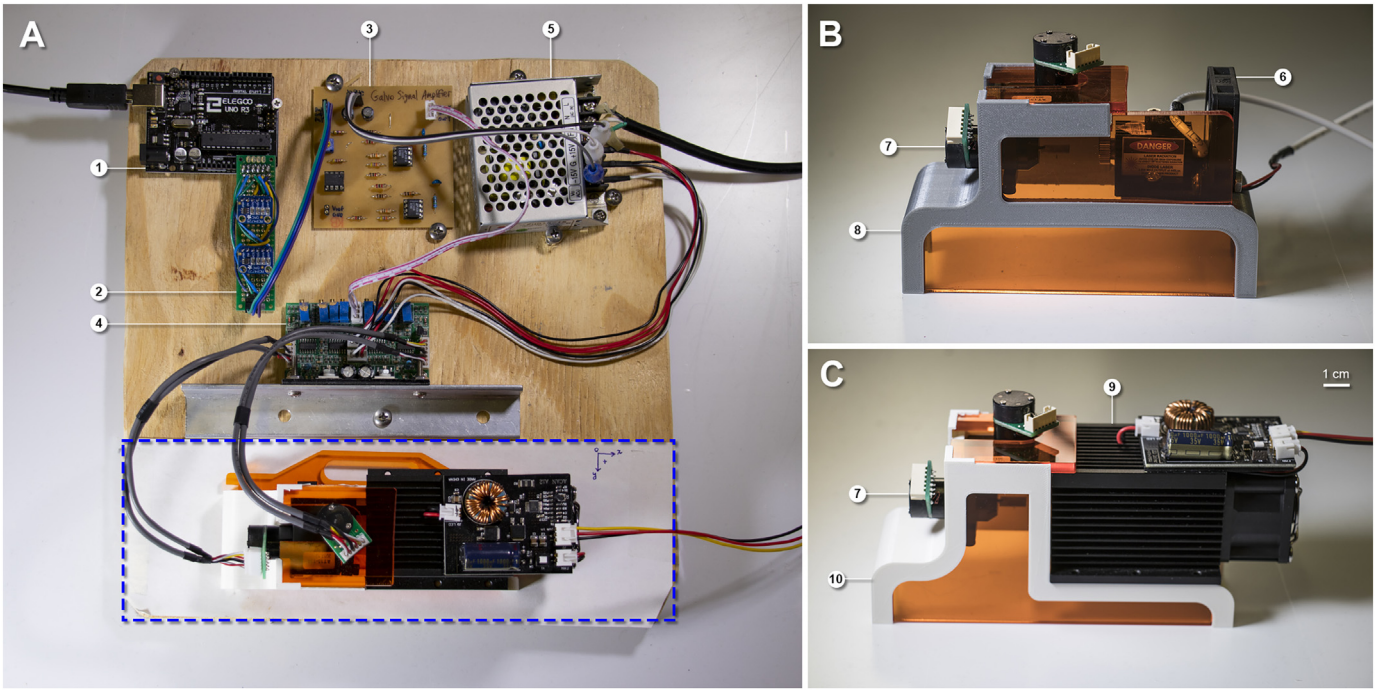

Fig. 1. Selective laser broiling system setup. A: The (1) Elegoo Uno R3 generates a digital signal that is converted into an analog signal via the (2) dual digital-to-analog converters. This analog voltage is amplified by the (3) custom amplifier circuit, before being transmitted to the (4) galvo mirror motor drivers that are equipped with a (5) power supply required for controlling the angle of the mirrors in order to precisely target the laser beam. B: The (6) 2 W laser diode is positioned in front of the (7) galvo mirrors; both are placed onto a (8) 3D-printed mount, which is inlaid with a 250–520 nm laser shielding acrylic. C: The (9) 5 W laser diode is positioned in front of a set of galvo mirrors by placing it onto a (10) custom 3D-printed mount. The blue-dashed region in A can accommodate systems B and C. (For interpretation of the references to color in this figure legend, the reader is referred to the web version of this article.)

mirrors was considered negligible in the cooking region.

Because the heat source exhibited some rectilinear distortion and sample thickness was non-uniform, a certain degree of circle diameter adjustment was required to achieve the desired trochoidal cooking pattern geometry. Using distance from the first incident mirror to the cooking platform (l, mm) and the thickness of the food sample (t, mm), the desired circle radius (R, inc) of the trochoidal cooking pattern was determined as follows:

$$R' = \left(\frac{l - t}{l}\right)R \tag{1}$$

where R' is the true analog value that should be used for a desired salmon sample thickness (t, mm). In order to quantify the energy delivered to the sample by adopting various cooking patterns, all pertinent variables needed to be expressed in terms of the aforementioned five independent variables defined in the computer code, namely circle radius (r), increment (j), scale (s), circle step (δ), and time delay (t). It should be noted that all five independent variables are unitless, since r and t are assigned integer values, and j, s, and δ are expressed as floating point numbers (to accommodate decimal points) in the Arduino software (Arduino, Ivrea, Italy).

Since the trochoidal—or interlaced circles—pattern is generated using the sine and cosine trigonometric functions, the repeating circles are interpolated by a series of points along a circle of the desired radius,

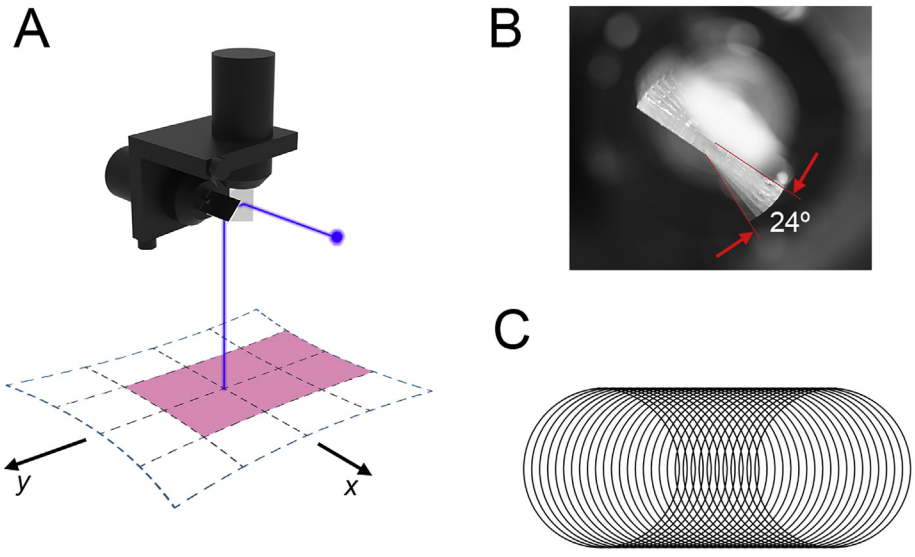

Fig. 2. Galvo mirror cooking schematic. A: Rendered image showing blue laser beam being reflected off a set of galvo mirrors to a 2D cooking plane; the blue dashed outline shows possible cooking region, while the magenta region indicates the operating region used for the experiments. B: Side view of one galvo mirror showing the 24° angle produced by the full 24 V electric potential difference. C: The trochoidal cooking pattern adopted in all experiments, where the diameter and density of circles produced by the laser beam, and laser motion speed can be adjusted. (For interpretation of the references to color in this figure legend, the reader is referred to the web version of this article.)

r. Number of points per circle (ξ) will affect the frequency (f) of the propagating circles as shown in Eqs. (2) and (3), respectively.

$$\xi = \frac{2\pi}{js} \tag{2}$$

$$f = \left[\left(\frac{t}{1000}\right)\xi\right]^{-1} = \frac{500js}{\pi t} \tag{3}$$

Period of oscillation (T) can be calculated by taking the inverse of frequency (f), while laser beam velocity can be computed using Eq. (4).

$$v = 2\pi rf = \frac{1000jsr}{t} \tag{4}$$

Calculating circle density (ρ) involves the use of Eq. (1) and the x scaling factor (s_x) presented in Section 2.2.3.

$$\rho = \frac{s_x}{\delta\xi} = \frac{js_x s}{2\pi\delta} \tag{5}$$

Finally, the energy per unit travel (ψ) and energy per unit area (ω) can be tabulated using the laser power (P), period of circle oscillation (T), points per circle (ξ), and the number of repetitions of the trochoidal pattern (n) as follows:

$$\psi = PT\rho n = P\left(\frac{\pi t}{500js}\right)\left(\frac{js_x s}{2\pi\delta}\right)n = \frac{Ps_x tn}{1000\delta} \tag{6}$$

$$\omega = \frac{\psi}{2r} = \frac{Ps_x tn}{2000\delta r} \tag{7}$$

2.3. Measuring sample surface color (L*a*b*) and thermal penetration depth

All images obtained in the present study were captured using a digital single-lens reflex camera (EOS 80D, Canon, Tokyo, Japan). An EF 100 mm macro lens (Canon, Tokyo, Japan) was used to capture close-up cross-sectional images, such as that shown in Fig. 3(A) and top views of the laser-heated salmon samples, as shown in Fig. 3(B). All images were taken in the "Canon Raw Version 2" mode, as this allowed us to white balance images in Adobe Photoshop CC; a white color swatch was placed in the same environment prior to shooting.

Cross-sectional images of the laser-heated salmon samples were analyzed in MATLAB. Color shift throughout the sample was assessed by comparing the cooked salmon color to the raw (uncooked) sections of the same sample. Depth of heat penetration was measured from the sample surface to the point within the sample at which the color from the heat-affected zone (HAZ) was within 10% of the threshold color (raw salmon color). This 10% limit was selected, since color variations within the raw portion of the salmon tended to fluctuate by 5–10% for each of the color values. Therefore, if the HAZ color was below 10%, this was interpreted as absence of color change due to heating. The method shown in Fig. 3(A) was used in determining the heat penetration depth (Section 3.2), while that depicted in Fig. 3(B) was adopted when conducting qualitative assessments. To reduce user measuring error, thermal penetration was measured seven times for each sample and averaged. The standard error was also tabulated by taking the standard deviation and dividing by the square of seven (number of values).

2.4. Measuring temperature

Maximum temperature was recorded at the bottom of the laser-heated salmon samples using a Leaton 4-Channel Digital Thermometer Thermocouple Sensor (Shenzhen DeXi Electronics Co, Shenzhen, China) with K-thermocouples (± 1 °C). The data-collecting heads of these thermocouples were placed in slots that were cut into the acrylic platform that supported the salmon sample, thus ensuring that four temperature readings could be made at the underside of the heated salmon. Temperature readings from the four probes were averaged and the standard error was calculated by taking the standard deviation and dividing by the square root of four. The depth of these temperature probes depended on the salmon sample thickness, which varied between 1 and 2 mm.

2.5. Determination of laser beam diameter

Beam quality and spatial energy distribution for the 2 W and 5 W diode lasers was examined using an FX-50 laser beam profiler (Ophir Optronics, Jerusalem, Israel). Major and minor beam diameters were measured for each laser at multiple z distances. The divergence angle for both diameters was calculated by linear interpolation between diameter measurements at varying z distances. An average was subsequently calculated and was adopted as each laser's divergence angle, which was used to calculate the beam diameter at the surface of the salmon sample.

Based on the experimental findings, the resulting Gaussian beam diameter of 0.97 mm and 2.95 mm was adopted for the 2 W and 5 W laser, respectively. Assuming these beam diameters, optical intensity (I)—also referred to as laser flux—can be calculated using the following equation:

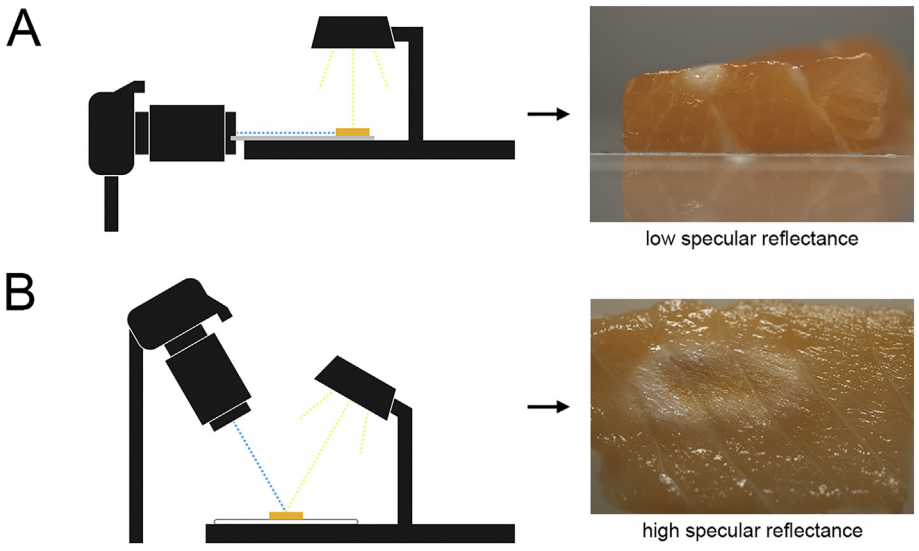

Fig. 3. Image capture schematic. A: The setup used for capturing cross-sectional images of the salmon sample (orange), where a light source is placed to minimize specular reflection (top lighting). Sample is positioned on a custom acrylic plate (gray) that ensures that the sample is located at the distance corresponding to the focal length of the camera. Blue dotted line shows the camera optical axis, while yellow dotted lines indicate the light source direction. B: The setup used for capturing top-view images, where a light source is placed on the same path as the camera optical axis, thereby increasing specular reflectance. (For interpretation of the references to color in this figure legend, the reader is referred to the web version of this article.)

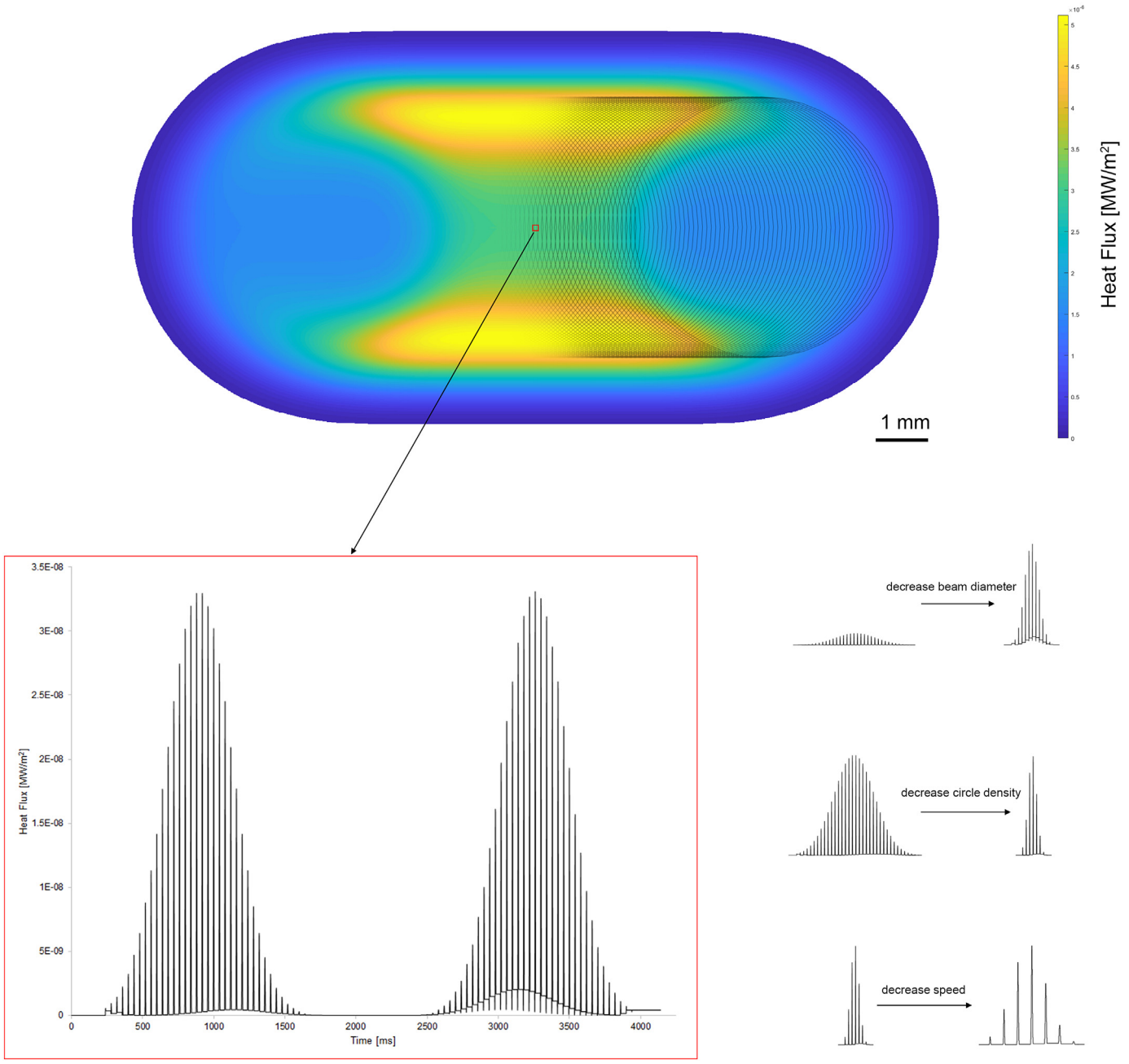

Fig. 4. MATLAB model of heat flux distribution on the food sample surface. The top graphic shows a heat map of the total heat flux at the surface of the laser-heated salmon sample (an overlay of half of the trochoidal heating pattern used in the tests is shown). The evolution of the heat flux over time for the central part of the heat-affected zone is shown in the bottom left image. Resultant heating profiles from altering variables are shown in the bottom right section.

$$I = \frac{P}{A} = \frac{4P}{\pi d^2} \tag{8}$$

The optical intensity of the 2 W laser diode (2.71 MW/m^2) calculated using the expression above is more than three times that of the 5 W laser diode (0.73 MW/m^2).

3. Results and discussion

3.1. Modeling laser heat flux distribution

Heating associated with selective laser broiling is different from that produced through conventional heating methods in that it results in "pulsed heating" (Blutinger et al., 2018a) as opposed to delivering continuous heat to a voxel—or 3D cube—of food. A MATLAB simulation was thus developed to better understand the heat flux profile that develops in a laser-heated food sample over time. This model traces the trochoidal heating pattern—used in the tests performed as a part of this investigation—while varying the circle radius, speed, circle density, and beam diameter in order to determine heat flux variance and distribution.

Fig. 4 shows a simplified model of the heating profile produced by delivering laser energy to the food sample in the previously described trochoidal pattern, where a radially symmetric Gaussian beam was assumed (as discussed in Section 2.5). Assuming that all other variables remain constant, decreasing the laser beam diameter will increase the variance and maximum beam flux, whereas decreasing the circle density will not affect maximum heat flux but will increase variance. Finally, decreasing the laser speed does not have an effect on either

variance or maximum heat. The two heating peaks shown in Fig. 4 correspond to the voxel "entering" and "exiting" the trochoidal pattern as the laser beam passes over the food sample. As the circle diameter increases, the distance between these two peaks will increase as well. It should be noted that all independent variables incorporated into the model will alter the shape and proximity of these heating peaks, and will thereby affect the heat variance and heat distribution within the salmon.

This method of "pulsed heating" must be employed for laser cooking, since the energy flux is two to three orders of magnitude higher than that produced by conventional heating methods used for food processing (Datta & Rakesh, 2013). The shape of each peak, comprised of a group of pulses, approximates the energy profile of the laser beam that is passing over the sample surface. As the optical center of the beam approaches the voxel of salmon meat, each successive pass of the beam will be registered as a pulse of heat until maximum heat flux is achieved, at precise optical alignment of the food voxel and the beam center. The temperature profile resulting from this temporal heat flux curve should approximate a similarly shaped smooth peak as well. By comparison, the heat flux profile from an oven operating at steady state should approximate more uniform heating profile, with surface heat flux roughly three orders of magnitude lower than the laser heat fluxes explored in this work (Datta & Rakesh, 2013). To achieve a similar degree of heat uniformity via SLB, a larger beam diameter with faster and more repetitive passes can be employed.

3.1.1. Effect of laser beam flux on cooking

Beam flux is determined by the laser power per unit area and is thus of particular importance in ensuring that salmon samples are heated effectively. This parameter is affected by the laser beam quality and collimation, as this will determine the energy delivered to the sample. However, higher beam flux will create a more variant energy profile with more pronounced peaks from "pulsed heating" (Blutinger et al., 2018a). As two lasers—5 W blue laser (more diffuse) and 2 W blue laser (less diffuse)—were used in the present study, they were analyzed and compared to assess the effects of beam flux on the salmon cooking results. Each laser beam was delivered to the salmon sample using the previously described trochoidal pattern. To compensate for the difference in power, the circle step was decreased by a factor of 2.5 for the 2 W laser (Fig. 5, right panel) to ensure that ω and ψ remained constant across trials.

Fig. 5 shows two different laser-exposed samples heated using the 2 W and 5 W laser; each have the same energy per area and energy per travel. Thus, the only difference between heating trials stemmed from the variations in the laser beam flux. Because the 2 W beam has a higher laser energy flux (2.71 MW/m^2), burning occurs much sooner (Fig. 5, left panel) than with the 5 W beam (0.73 MW/m^2). While slight burning did occur in the 5 W beam test (Fig. 5, right panel), this was attributed to the edge effects of the beam, as opposed to the peak energy at the center of the beam. The HAZ of the 5 W beam is also much greater, as can be seen in Fig. 5, where larger whitish area around the edges of the trochoidal pattern can be discerned, which extends further than in the sample subjected to the 2 W laser beam. Since the major difference between these two tests stems from the change in energy variance, the obtained results demonstrate that higher beam flux causes the food sample to burn sooner and have a poor cooking quality. Burning due to high-intensity laser energy was also found during the baking and browning of dough products via laser (Blutinger et al., 2018a, 2018b).

3.2. Assessing heat penetration depth via color analysis

Salmon sample thickness has a significant effect on depth of heat penetration. In the present investigation, heat dispersion, which was more prominent in thicker samples, made it more difficult to fully cook the salmon meat. Because thinner salmon samples have less mass, more of the heat builds up and cooks the entire salmon cross-section more effectively (Wojtkowiak, 2014). Cooking thicker samples resulted in a steady color gradient from off-white (cooked) to pink/orange (raw), which made it more difficult to determine thermal penetration depth.

To more accurately calculate the depth of heat penetration in the laser-heated samples, a software tool was developed. Laser-heated samples produced a color gradient from off-white (cooked) to orange (raw) with increasing depth from the surface. This made it difficult to accurately determine the heat-affected zone (HAZ) for each salmon sample. To mitigate this issue, a custom script was developed in MATLAB, thus ensuring that a more quantitative (and thus more accurate) method was adopted to measure heat penetration depth. The script allows a user to (1) analyze the pixel color value along a specified line across the salmon sample, (2) select a threshold color as a means of comparison, and (3) determine the depth of heat penetration (Fig. 6). If salmon color is within 10% of the threshold color for any of the three color intensities (L^*, a^*, or b^*), this point is adopted as the depth of heat penetration. This method of measurement was used to calculate the values reported in Sections 3.2.1–3.2.4. It should also be noted that all heat penetration depth tests that yielded findings depicted in Figs. 7–10 were conducted using the 2 W blue laser diode.

Single-factor experiments were devised in Sections 3.2.1–3.2.4 to develop an understanding on the effect each laser parameter has on the thermal penetration of Atlantic salmon. Further data collection is required to expand the richness of the dataset, while further analysis (e.g. response surface methodology or symbolic regression) could develop understanding of parameter interactions (Baş & Boyacı, 2007; Blutinger et al., 2018a).

Fig. 5. Effect of laser beam flux on the salmon cooking results. Left panel: 1 mm thick salmon sample heated using a trochoidal cooking pattern with P = 2 W, r = 2.5 mm, T = 0.04 s, ρ = 200 rev/mm, and I = 2.71 MW/m^2. Right panel: 1 mm thick salmon sample heated using the same trochoidal cooking pattern except P = 5 W, ρ = 80 rev/mm, and I = 0.73 MW/m^2. Both patterns yield the same ω (3.2 kJ/m) and ψ (16 MJ/m).

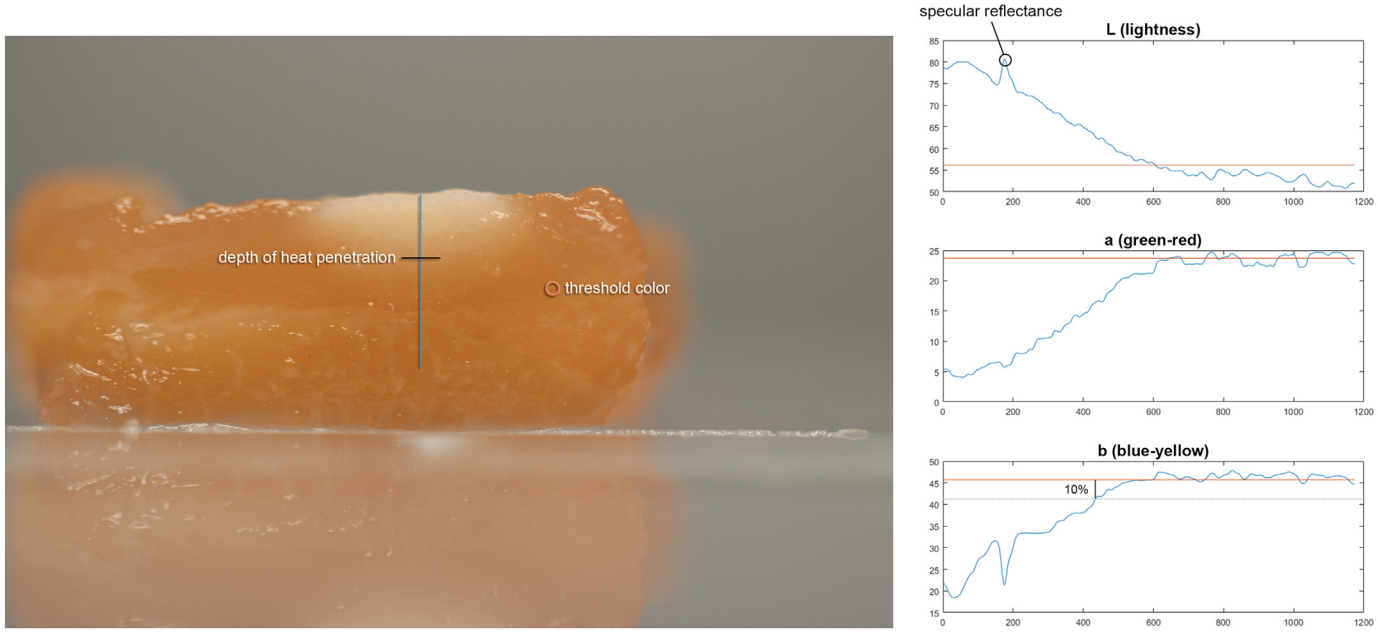

Fig. 6. Method used to determine heat penetration depth in salmon samples. The pixel colors are calculated along a user-specified line on the cross-sectional view of a laser-heated piece of salmon (left panel). Heat penetration depth is determined as the distance from the sample surface to the point where the color is within 10% of the threshold color specified by the user.

3.2.1. Effect of circle diameter on thermal penetration

One of the parameters that can be altered to affect the cooking depth is the diameter of the repeating circle comprising the trochoidal cooking pattern. Increasing the circle diameter—while keeping other variables constant—decreases the energy per unit area (ω), without affecting the energy per unit travel (ψ), which remained constant at 1.36 kJ/m throughout these trials. By increasing the diameter of the interlaced circles, the speed of the moving laser will also increase due to the larger step size between points along the interpolated circle path.

Fig. 7 shows the effect of circle diameter variation on the heat penetration depth in the heated samples. Even though thermal penetration does not exhibit a clear relationship with ω, as expected, there is a downward trend as energy per unit area decreases. When less laser energy is delivered to the food sample, less heat is available to denature protein and induce a color change in the salmon. At a circle diameter of 9 mm (ω = 0.15 MJ/m^2), a slight color change can be seen in the cross-sectional view of the salmon sample. However, it is insufficient to surpass 10% of the threshold color.

At higher ω ($\geq$0.68 MJ/m^2), a more pronounced indentation at the center of the heated sample can be noticed on the salmon sample surface. This effect could be due to the high heat density and more consistent heat distribution over time. This surface indentation is consistent

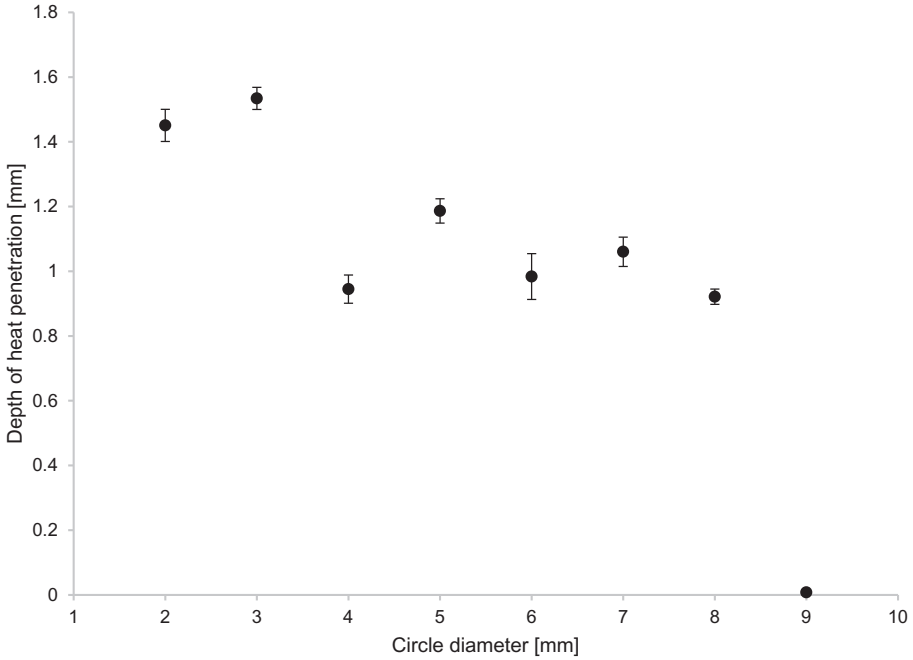

Fig. 7. Depth of heat penetration as a function of circle diameter produced by the 2 W laser. As circle diameter increases, the depth of heat penetration steadily decreases. Error bars represent standard error for the heat penetration depth based on seven measurements performed within the same cooking trial.

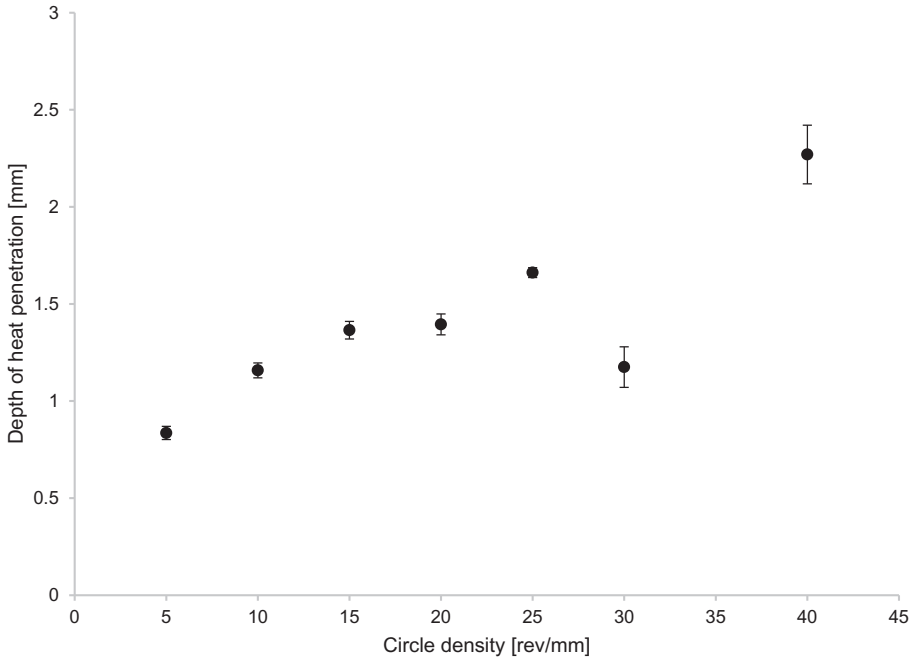

Fig. 8. Depth of heat penetration as a function of circle density produced by the 2 W laser. As the circle density increases, the heat penetration depth steadily increases. Error bars represent standard error for the depth of heat penetration based on seven measurements conducted as a part of the same cooking trial.

with CO_2 laser browning of dough, where excessive laser heat resulted in a deepening effect on the food surface (Blutinger et al., 2018a). During the cooking trial in which a circle of 1 mm diameter (ω = 1.34 MJ/m^2) was employed, significant burning occurred at the center of the HAZ, along with a significant indentation due to heating. Similar to laser-induced dough burning, this could be due to rapid water evaporation (Blutinger et al., 2018a).

3.2.2. Effect of circle density on thermal penetration

Circle density has a clearer effect on heat penetration depth of laser-heated salmon than does circle diameter. As this variable is directly proportional to ψ and ω, it exhibits nearly linear relationship with the heat penetration depth (Fig. 8). At a circle density of 40 and 50 rev/mm, the surface of the laser-heated salmon started to burn. These laser parameters create heating effects that contribute to fast water evaporation. Hence, if the radiant heat does not penetrate the sample cross-section sufficiently, the effect is similar to hot air heating in an oven (Datta & Rakesh, 2013). This evaporative drying could be dehydrating the sample, thereby making it more susceptible to burning due to the lower moisture content, which tends to result from longer heat exposure (Takahashi & Khan, 1987).

3.2.3. Effect of repetitions on thermal penetration

In further tests, the same trochoidal pattern was repeated successively to assess the degree to which repetitive heating can increase heat penetration depth. The previously described interlaced circles pattern

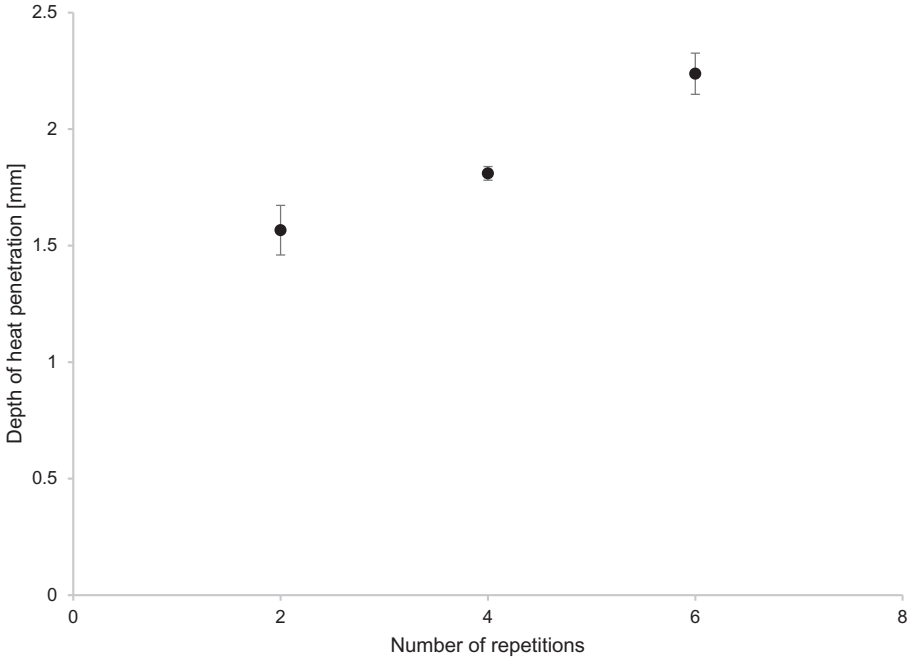

Fig. 9. Depth of heat penetration as a function of laser pattern repetition using the 2 W laser. As the number of cooking pattern repetitions increases, the heat penetration depth steadily increases. Error bars represent standard error for the depth of heat penetration based on seven measurements performed as a part of the same cooking trial.

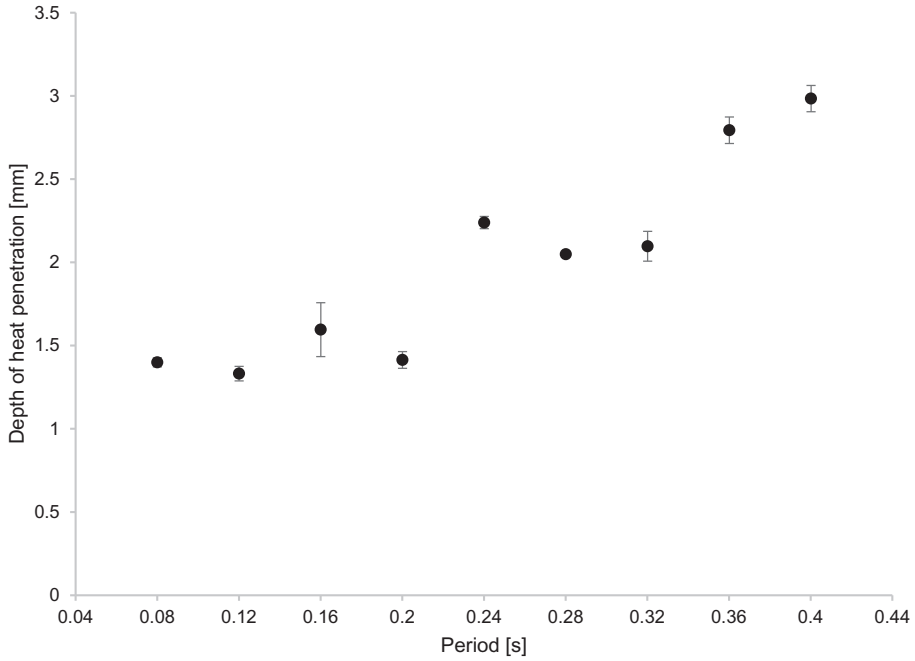

Fig. 10. Depth of heat penetration as a function of trochoid period when using the 2 W laser. As the period of the trochoid pattern increases, the depth of heat penetration increases. Error bars represent standard error for the heat penetration depth based on seven measurements performed within the same cooking trial.

with a 5 mm diameter, 0.04 s period, and 16.9 rev/mm circle density was repeated two, four, and six times. Each successive repetition resulted in a higher depth of heat penetration. Fig. 9 shows the direct relationship between the laser energy penetration depth and the number of successive laser pattern repetitions delivered to the same sample.

Qualitatively, heating the same sample area with the 2 W blue laser expands the HAZ on the sample surface and further toughens and texturizes the meat. With each successive heating trial, the salmon loses moisture, thus becoming less tender, making it less desirable as a final cooked product (Kong, Tang, Lin, & Rasco, 2008). Meat that is heated at a lower temperature over a longer period of time tends to produce a more tender final cooked product than meat that is cooked at high heat for a short period (Bertola, Bevilacqua, & Zaritzky, 1994; Machlik & Draudt, 1963; Penfield & Meyer, 1975). As such, repetitive laser cooking at high speed (lower energy intensity) as opposed to cooking the food with a slower laser speed should provide better meat tenderness, which is an important quality criteria in cooked food products (Bertola et al., 1994).

3.2.4. Effect of trochoid period on thermal penetration

Finally, heat penetration depth is directly proportional to the interlaced circles pattern period. By increasing the time delay (t), the speed of the moving laser decreases, thereby increasing the period (T) of the moving beam, as well as the energy per area and energy per travel. This results in greater heat penetration depth, since the laser heats the salmon sample for a longer period as it travels across the food surface.

Due to the salmon surface being exposed to a greater radiant heat flux, more energy is being absorbed by the food sample, causing it to heat up and conduct heat through the depth profile, thus contributing to a larger HAZ. From the image shown in Fig. 10, it can be seen that the relationship between the trochoid period and heat penetration depth is fairly linear. Since the trochoid period is linearly related to the energy being delivered to the food, it stands to reason that a linear increase in total energy will correspond to a linear increase in temperature and thermal penetration (Borgnakke & Sonntag, 2013).

As period of the trochoidal pattern increased (i.e., laser speed decreased), the texture of the heated salmon seemed to become firmer as well. Consequently, achieving a clean cut through the salmon samples that cooked at a higher ω and ψ became increasingly difficult. This change in texture could also be due to loss of moisture resulting from the longer cooking time (Kong, Tang, Rasco, & Crapo, 2007). Extending the cooking time and thus laser energy exposure also resulted in more noticeable sweating, as moisture was released from the HAZ (Bircan & Barringer, 2002). When periods of $T \geq 0.28$ s ($\omega = 1.86$ MJ/m^2 and $\psi = 9.49$ kJ/m) were adopted in the laser heating trials, audible popping sounds could be heard, which could be due to high heat exposure and water evaporation.

3.3. Effect of salmon thickness on heating

Food sample thickness has a notable effect on laser heating (Blutinger et al., 2018b), which likely explains some of the nonlinearity evident in Figs. 7–10. Thus, to assess the effect of thermal diffusion within the salmon, the same trochoidal cooking pattern was used to cook a 4.5 mm thick sample and a 1 mm sample. After laser exposure, a slight surface indentation could be observed on the thicker piece of salmon due to muscle shrinkage (Bircan & Barringer, 2002). While both samples were fully cooked through, the thinner sample (Fig. 5, right panel) showed signs of burning on the surface, which could be due to the greater amount of heat buildup. Similarly, Blutinger et al. (2018b) found that thinner dough products tend to laser cook faster due to smaller volume and quicker heat transfer (Borgnakke & Sonntag, 2013), which should match intuition.

Fig. 11 presents two heated test samples (of 1.5–2 mm thickness) that exhibited some visual traits that the thicker test samples (discussed in Section 3.2) did not. First, these samples were heated using the 5 W laser—as opposed to the 2 W laser—which provided more diffuse heating and produced less burning. Second, a brown crust formed on the surface of the laser-heated samples, as shown in Fig. 11(A) and (C), which is a very desirable texture that is more common when pan frying salmon (Larsen, Quek, & Eyres, 2011). This brown crust probably formed due to increased dehydration (Larsen et al., 2011), and could also be attributed to the Maillard reaction (Haard, 1992). Third, a higher amount of white moist coagulum can be seen in these samples. It

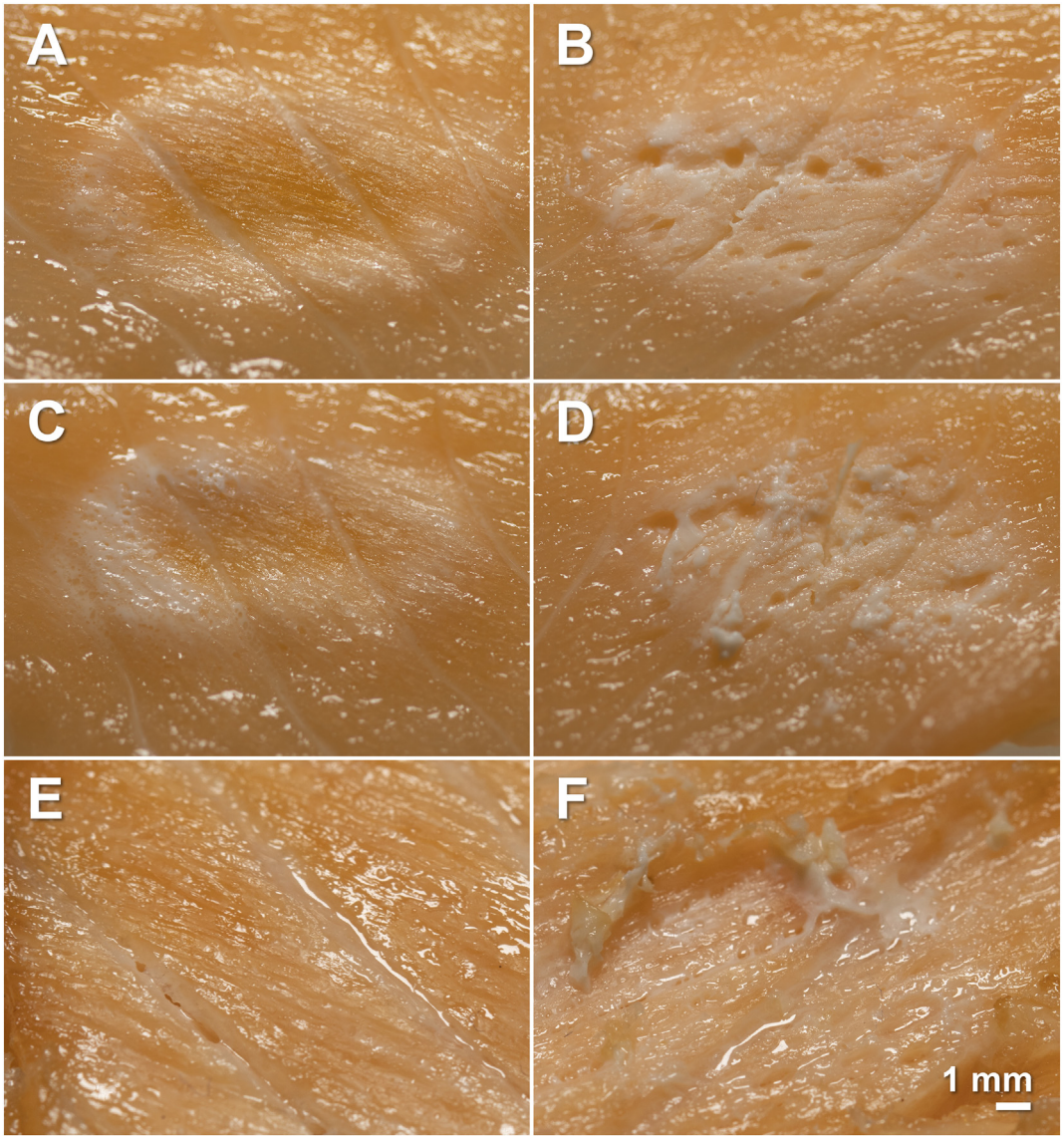

Fig. 11. Comparing cook quality of laser-broiled and oven-broiled test samples. A: Top view of first laser-broiled sample (ω = 0.89 MJ/m^2). B: Bottom view of same laser-broiled sample (ω = 0.89 MJ/m^2). C: Top view of second laser-broiled sample at ω = 1.00 MJ/m^2. D: Bottom view of same laser-broiled sample (ω = 1.00 MJ/m^2). E: Top view of oven-broiled sample (3 min at 500 F). F: Bottom view of same oven-broiled sample (3 min at 500 F). Samples A-D were heated using the 5 W laser and the same energy per travel (ψ = 7.99 kJ/m). The spherical pockets shown in the images denoted as B and D are from the thermistors.

is most apparent in the image shown in Fig. 11(C), which could suggest a slower heat penetration and thus more even cooking rate (Charley & Goertz, 1958). Last, the texture and change in surface gloss due to cooking, as well as the more flaky texture of the laser-exposed samples, can be noted in Fig. 11. This flaky appearance results from weak muscle bonds, which are broken down when the muscle is sufficiently cooked (Dunajski, 1980).

3.4. Effect of repeated exposure on maximum internal temperature

To achieve a food-safe cooking temperature (62.8 °C), the previously described trochoidal cooking pattern was repeated multiple times while keeping all heating parameters constant (r = 2.5 mm, j = 0.1, s = 1.57, δ = 0.1, t = 1 ms). For this experiment, only the 2 W laser was used in four repetitions, and temperature was recorded at the bottom of the heated salmon sample (Fig. 12).

With each successive pass of the laser over the same salmon sample area, the internal temperature of the sample steadily increased. Fig. 12 shows this temperature increase between successive blue laser passes. After the third pass of the laser, an internal food temperature of 69.8 °C was measured, which is well above the food-safe temperature of 62.8 °C. Brown crust formed on the salmon surface, which also occurred when the 5 W laser was used for heating (Section 3.3). This 2 mm thick Atlantic salmon sample reached a final cooked temperature of 74.5 °C and exhibited a flaky texture, both of which are qualities of properly cooked salmon (Dunajski, 1980).

3.5. Energy effects on maximum internal sample temperature

Over multiple experiments, the energy per unit area (ω) and energy per unit length (ψ) were varied while maximum temperature measurements were recorded at the bottom of the heated salmon samples. These tests were conducted using both 2 W and 5 W blue laser diode (Fig. 13) to assess to what degree minimum food-safe temperatures (62.8 °C), as determined by USDA FSIS (2015), could be reached in the heated samples. Initially, salmon samples were at the ambient temperature of 21–25 °C. However, this variance should not have a significant effect on the maximum heating temperature recorded within

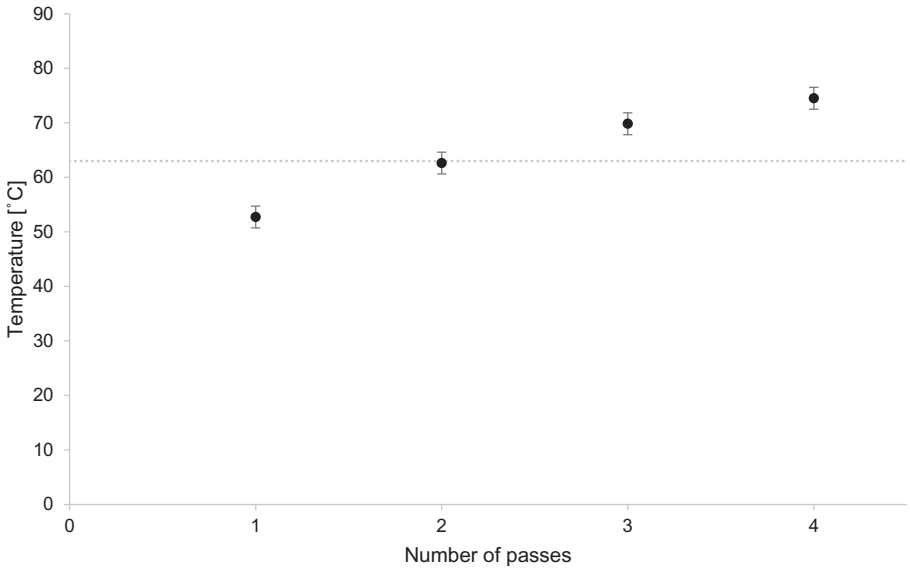

Fig. 12. Change in maximum salmon temperature due to repeated exposure to 2 W laser energy. After two passes, internal salmon temperature exceeded the minimum temperature (62.8 °C) required by the food safety standards imposed by the USDA FSIS. Error bars represent standard error for the average temperature based on four thermistor readings performed within the same cooking trial.

the sample (Blutinger et al., 2018b).

Placement of the temperature sensors does help explain the large standard error visible in the graphs shown in Fig. 13. In Fig. 11(B) and (D), the spherical imprints made by the temperature probes, which were spaced out along the length of the laser's trochoidal cooking path, are clearly visible. Since greater total laser energy is delivered towards the center of the heating path (Fig. 4), thermistors along the edges of the cooking path recorded a lower temperature.

Aside from the discernable error bars in the graphs shown in Fig. 13, a clear trend can be noticed. Maximum internal temperature of the cooked salmon samples seems to plateau at around 77–80 °C, irrespective of the ω and ψ values, indicating that thermal equilibrium is reached (Borgnakke & Sonntag, 2013). This equilibrium begins to take effect when $\omega > 1\ \mathrm{MW/m^2}$ and $\psi > 8\ \mathrm{kJ/m}$. At these thresholds the ambient cooling rate of the sample matches the heat provided by the laser, and no further increase in temperature can be achieved. Establishing the point at which adding more energy into the food system contributes to no further increase in temperature is important. Understanding this point of thermal equilibrium allows the cooking process to be accelerated and more economical by optimizing laser energy

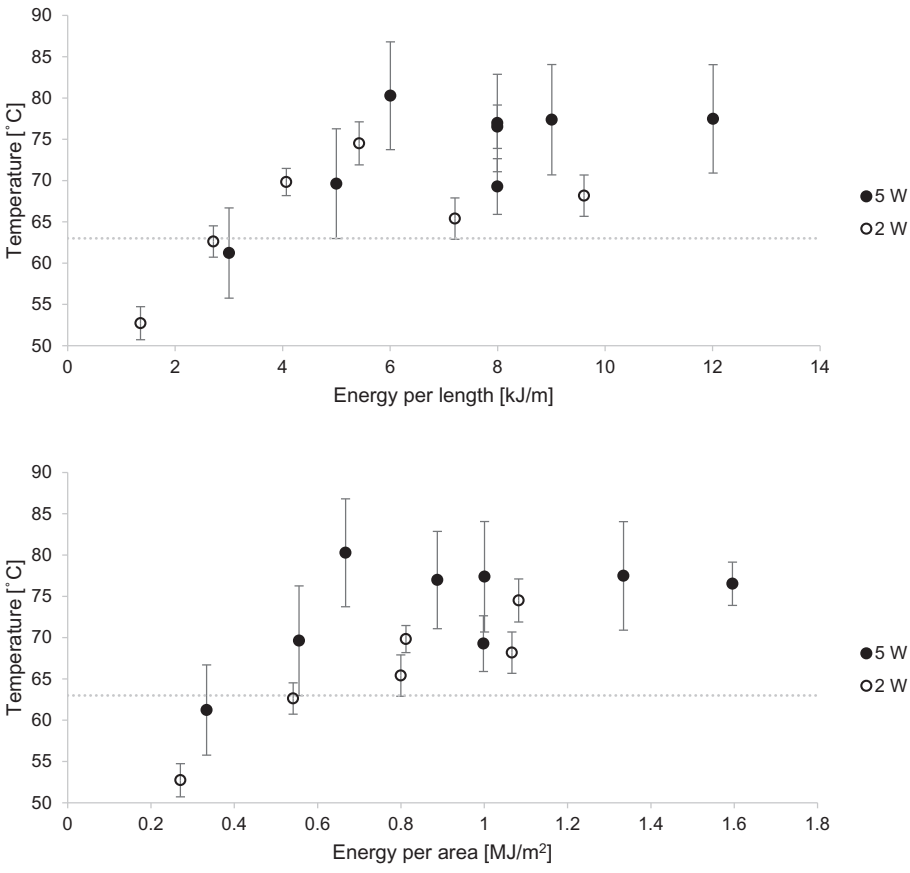

Fig. 13. Maximum internal temperature of the salmon sample obtained in different heating trials. Maximum internal salmon temperature was assessed as a function of energy per length (top) and energy per area (bottom). The dotted line shows the minimum temperature for food safety set by the USDA FSIS (62.8 °C). Error bars represent standard error for the average temperature based on four measurements performed within the same cooking trial.

utilization.

3.6. Comparing laser-broiled and oven-broiled salmon fillets

A final test was performed to compare laser broiling to a more conventional cooking method—oven broiling. A fillet of salmon was broiled for 3 min at 500 F in a toaster oven, providing the sample sufficient time to achieve full protein denaturation. Fig. 11(E) and (F) provide a top and bottom view of the oven-broiled sample, respectively. During oven broiling, the salmon fillet developed a brown crust along its edges (left portion of Fig. 11E) and underside (top portion of Fig. 11F), a firm and flaky texture, and a familiar off-white (cooked) color. For laser-broiled samples, this brown crusting originates from the center of the heat-affected region (Fig. 11A and C), instead of from the edges of the sample. Reason for the difference in the origination of the brown crust can be attributed to differences in concentrated heat flux. Meats can exhibit a very high difference in temperature within the same sample during oven-roasting (Marshall, Wood, & Patton, 1960). Traits that are similar between the two samples include the presence of white coagulum on the underside of both test samples (Fig. 11, D and F), a similar off-white color for the cooked portion of the fillet, and brown crust texture along areas with more concentrated heat flux.

4. Conclusions

Our selective laser broiling (SLB) system provides compact, software-controlled cooking with a degree of precision and temporal control unrivaled by conventional cooking methods. Full protein denaturation is achieved in salmon fillets of 1–3 mm, proving that “pulsed heating” via SLB works most effectively in a food layered manufacture application and where foodstuffs are thin and require precise heating. To achieve desirable texture and food safe cooking temperatures with a trochoidal cooking pattern, an energy per area of 0.6–1.2 MJ/m^2 and an energy per unit length of 5–10 kJ/m should be used. We also found that circle density, period, and number of repetitions are linearly related to depth of heat penetration, while circle diameter is inversely proportional to thermal penetration. Use of a diffuse high-powered laser (< 1 MW/m^2), at faster speeds, with repetitive exposure emerged as a more effective way to laser cook Atlantic salmon (*Salmo salar*). Future research will be needed to look more deeply at the effect that laser parameters have on cooking loss (moisture), nutritional content (digestibility), and macro structure for laser-heated foods. Finally, sensory tests are crucial to evaluate the organoleptic acceptance of laser-cooked products.

Acknowledgements

This work was supported in part by Columbia University's SEAS Interdisciplinary Research Seed (SIRS) funding program.

References

Anderson, S. (2001). Salmon color and the consumer. *International institute of fisheries economics and trade*. Retrieved from https://ir.library.oregonstate.edu/concern/conference_proceedings_or_journals/9s1616848?locale=en.

Barbanti, D., & Pasquini, M. (2005). Influence of cooking conditions on cooking loss and tenderness of raw and marinated chicken breast meat. *LWT - Food Science and Technology, 38*(8), 895–901. https://doi.org/10.1016/j.lwt.2004.08.017.

Barrett, D. M., Beaulieu, J. C., & Shewfelt, R. (2010). Color, flavor, texture, and nutritional quality of fresh-cut fruits and vegetables: Desirable levels, instrumental and sensory measurement, and the effects of processing. *Critical Reviews in Food Science and Nutrition, 50*(5), 369–389. https://doi.org/10.1080/10408391003626322.

Baş, D., & Boyacı, İ. H. (2007). Modeling and optimization I: Usability of response surface methodology. *Journal of Food Engineering, 78*(3), 836–845. https://doi.org/10.1016/J.JFOODENG.2005.11.024.

Bertola, N. C., Bevilacqua, A. E., & Zaritzky, N. E. (1994). Heat treatment effect on texture changes and thermal denaturation of proteins in beef muscle. *Journal of Food Processing and Preservation, 18*(1), 31–46. https://doi.org/10.1111/j.1745-4549.1994.tb00240.x.

Bircan, C., & Barringer, S. A. (2002). Determination of protein denaturation of muscle foods using the dielectric properties. *Journal of Food Science, 67*(1), 202–205. https://doi.org/10.1111/j.1365-2621.2002.tb11384.x.

Blutinger, J. D., Meijers, Y., Chen, P. Y., Zheng, C., Grinspun, E., & Lipson, H. (2018a). Characterization of CO2 laser browning of dough. *Innovative Food Science & Emerging Technologies*. https://doi.org/10.1016/J.IFSET.2018.11.013.

Blutinger, J. D., Meijers, Y., Chen, P. Y., Zheng, C., Grinspun, E., & Lipson, H. (2018b). Characterization of dough baked via blue laser. *Journal of Food Engineering, 232*, 56–64. https://doi.org/10.1016/j.jfoodeng.2018.03.022.

Borgnakke, C., & Sonntag, R. E. (2013). Fundamentals of thermodynamics (8th ed., p. 6). Hoboken, NJ: Don Fowley. Retrieved from http://www.academia.edu/13057225/Book_-_Fundamentals_Of_Thermodynamics_8th_edition.

Carpenter, C. E., Cornforth, D. P., & Whittier, D. (2001). Consumer preferences for beef color and packaging did not affect eating satisfaction. *Meat Science, 57*(4), 359–363. Retrieved from http://www.ncbi.nlm.nih.gov/pubmed/22061707.

Charley, H., & Goertz, G. E. (1958). The effects of oven temperature on certain characteristics of baked salmon. *Journal of Food Science, 23*(1), 17–24. https://doi.org/10.1111/j.1365-2621.1958.tb17533.x.

Chen, P. Y., Blutinger, J. D., Meijers, Y., Zheng, C., Grinspun, E., & Lipson, H. (2019). Visual modeling of laser-induced dough browning. *Journal of Food Engineering, 243*, 9–21. https://doi.org/10.1016/J.JFOODENG.2018.08.022.

Datta, A. K., & Rakesh, V. (2013). Principles of microwave combination heating. *Comprehensive Reviews in Food Science and Food Safety, 12*(1), 24–39. https://doi.org/10.1111/j.1541-4337.2012.00211.x.

Dissing, B. S., Nielsen, M. E., Ersbøll, B. K., & Frosch, S. (2011). Multispectral imaging for determination of Astaxanthin concentration in Salmonids. *PLoS ONE, 6*(5), e19032. https://doi.org/10.1371/journal.pone.0019032.

Dunajski, E. (1980). Texture of fish muscle. *Journal of Texture Studies, 10*(4), 301–318. https://doi.org/10.1111/j.1745-4603.1980.tb00862.x.

Fukuchi, K., Jo, K., Tomiyama, A., & Takao, S. (2012). Laser cooking. *Proceedings of the ACM multimedia 2012 workshop on multimedia for cooking and eating activities - CEA. Vol. 12. Proceedings of the ACM multimedia 2012 workshop on multimedia for cooking and eating activities - CEA* (pp. 55–). New York, New York, USA: ACM press. https://doi.org/10.1145/2390776.2390788.

Gormley, T. (1992). A note on consumer preference of smoked salmon colour. *Irish Journal of Agricultural and Food Research,* 31.

Haard, N. F. (1992). Biochemistry and chemistry of color and color changes in seafoods. In G. J. Flick, & R. E. Martin (Eds.). *Advances in seafood biochemistry: Composition and quality* (pp. 305–360). Lancaster, PA: Technomic Publishing Company, Inc.

Hertafeld, E., Zhang, C., Jin, Z., Jakub, A., Russell, K., Lakehal, Y., ... Lipson, H. (2018). *Multi-material three-dimensional food printing with simultaneous infrared cooking. 3D Printing and Additive Manufacturing, 3dp. 2018*, 0042. https://doi.org/10.1089/3dp.2018.0042.

Jeremiah, L. E., Carpenter, Z. L., & Smith, G. C. (1972). Beef color as related to consumer acceptance and palatability. *Journal of Food Science, 37*(3), 476–479. https://doi.org/10.1111/j.1365-2621.1972.tb02667.x.

Kong, F., Tang, J., Lin, M., & Rasco, B. (2008). Thermal effects on chicken and salmon muscles: Tenderness, cook loss, area shrinkage, collagen solubility and microstructure. *LWT - Food Science and Technology, 41*(7), 1210–1222. https://doi.org/10.1016/J.LWT.2007.07.020.

Kong, F., Tang, J., Rasco, B., & Crapo, C. (2007). Kinetics of salmon quality changes during thermal processing. *Journal of Food Engineering, 83*(4), 510–520. https://doi.org/10.1016/J.JFOODENG.2007.04.002.

Kong, F., Tang, J., Rasco, B., Crapo, C., & Smiley, S. (2007). Quality changes of salmon (oncorhynchus gorbuscha) muscle during thermal processing. *Journal of Food Science, 72*(2), S103–S111. https://doi.org/10.1111/j.1750-3841.2006.00246.x.

Larsen, D., Quek, S.-Y., & Eyres, L. (2011). Evaluating instrumental colour and texture of thermally treated New Zealand king Salmon (Oncorhynchus tshawytscha) and their relation to sensory properties. *LWT - Food Science and Technology, 44*(8), 1814–1820. https://doi.org/10.1016/J.LWT.2011.03.018.

Lentz, R. R., Pesheck, P. S., Anderson, G. R., DeMars, J., & Peck, T. R. (1995). *US 5382441 A*.

Lipson, H., & Kurman, M. (2013). Fabricated: The new world of 3D printing. Retrieved from https://books.google.com/books?hl=en&lr=&id=MpLXWHp-srIC&oi=fnd&pg=PA1&dq=3d+food+printing&ots=Z3bZySJ3_H&sig=J0B9KCDystLtS9v1aa-Ub2wECzg#v=onepage&q=3dfood printing&f=false.

Lipton, J. I., Cutler, M., Nigl, F., Cohen, D., & Lipson, H. (2015). Additive manufacturing for the food industry. *Trends in Food Science & Technology, 43*(1), 114–123. https://doi.org/10.1016/J.TIFS.2015.02.004.

Machlik, S. M., & Draudt, H. N. (1963). The effect of heating time and temperature on the shear of beef semitendinosus muscle. *Journal of Food Science, 28*(6), 711–718. https://doi.org/10.1111/j.1365-2621.1963.tb01678.x.

Mancini, R. A., & Hunt, M. C. (2005). Current research in meat color. *Meat Science, 71*(1), 100–121. https://doi.org/10.1016/J.MEATSCI.2005.03.003.

Marshall, N., Wood, L., & Patton, M. B. (1960). Cooking choice grade, top round beef roasts. *Journal of the American Dietetic Association, 36*, 341–345. Retrieved from http://www.ncbi.nlm.nih.gov/pubmed/14421547.

Ofstad, R., Egelandsdal, B., Kidman, S., Myklebust, R., Olsen, R. L., & Hermansson, A.-M. (1996). Liquid loss as effected by post mortem ultrastructural changes in fish muscle: Cod (Gadus morhua L) and Salmon (Salmo salar). *Journal of the Science of Food and Agriculture, 71*(3), 301–312. https://doi.org/10.1002/(SICI)1097-0010(199607)71:3<301::AID-JSFA583>3.0.CO;2-0.

Penfield, M. P., & Meyer, B. H. (1975). Changes in tenderness and collagen of beef semitendinosus muscle heated at two rates. *Journal of Food Science, 40*(1), 150–154. https://doi.org/10.1111/j.1365-2621.1975.tb03758.x.

Pope, R. M., & Fry, E. S. (1997). Absorption spectrum (380–700 nm) of pure water II integrating cavity measurements. *Applied Optics, 36*(33), 8710–8723. https://doi.org/

10.1364/AO.36.008710.
Sandu, C. (1986). Infrared radiative drying in food engineering: A process analysis. *Biotechnology Progress, 2*(3), 109–119. https://doi.org/10.1002/btpr.5420020305.
Sigurgisladottir, S., Hafsteinsson, H., Jonsson, A., Lie, O., Nortvedt, R., Thomassen, M., & Torrissen, O. (1999). Textural properties of raw salmon fillets as related to sampling method. *Journal of Food Science, 64*(1), 99–104. https://doi.org/10.1111/j.1365-2621.1999.tb09869.x.
Singh, I. (2011). US9107434B2. Retrieved from https://patents.google.com/patent/US9107434B2/en.
Sun, J., Zhou, W., Yan, L., Huang, D., & Lin, L. (2018). Extrusion-based food printing for digitalized food design and nutrition control. *Journal of Food Engineering, 220*, 1–11. https://doi.org/10.1016/J.JFOODENG.2017.02.028.
Takahashi, Y., & Khan, M. A. (1987). Impact of infrared broiling on the thiamin and riboflavin retention and sensory quality of salmon steaks for foodservice use. *Journal of Food Science, 52*(1), 4–6. https://doi.org/10.1111/j.1365-2621.1987.tb13961.x.
USDA (2018). Food composition databases show foods – Fish, salmon, Atlantic, wild, raw. Retrieved from https://ndb.nal.usda.gov/ndb/foods/show/303440?manu=&fgcd=&ds=&q=Fish,salmon,Atlantic,wild,raw.
USDA FSIS (2015). Safe minimum internal temperature Chart. Retrieved September 7, 2018, from https://www.fsis.usda.gov/wps/portal/fsis/topics/food-safety-education/get-answers/food-safety-fact-sheets/safe-food-handling/safe-minimum-internal-temperature-chart/CT_Index.
Wojtkowiak, J. (2014). Lumped thermal capacity model. *Encyclopedia of thermal stresses* (pp. 2808–2817). Dordrecht: Springer Netherlands. https://doi.org/10.1007/978-94-007-2739-7_393.
Yagiz, Y., Kristinsson, H. G., Balaban, M. O., Welt, B. A., Ralat, M., & Marshall, M. R. (2009). Effect of high pressure processing and cooking treatment on the quality of Atlantic salmon. *Food Chemistry, 116*(4), 828–835. https://doi.org/10.1016/J.FOODCHEM.2009.03.029.
Yang, F., Zhang, M., & Bhandari, B. (2017). Recent development in 3D food printing. *Critical Reviews in Food Science and Nutrition, 57*(14), 3145–3153. https://doi.org/10.1080/10408398.2015.1094732.
Zoran, A., & Coelho, M. (2011). *Cornucopia: The concept of digital gastronomy. vol. 44(5)*, MIT Press425–431. Retrieved from http://muse.jhu.edu/journals/len/summary/v044/44.5.zoran.html.